Synthesis, Morphology, and Sensory Applications of Multifunctional Rod−Coil−Coil Triblock Copolymers and Their Electrospun Nanofibers

Yu-Cheng Chiu,[†] Yougen Chen,[‡] Chi-Ching Kuo,[§] Shih-Huang Tung,[⊥] Toyoji Kakuchi,[*,‡] and Wen-Chang Chen[*,†]

[†]Department of Chemical Engineering and [⊥]Institute of Polymer Science and Engineering, National Taiwan University, Taipei 10617, Taiwan

[‡]Division of Biotechnology and Macromolecular Chemistry, Graduate School of Engineering, Hokkaido University, Sapporo 060-8628, Japan

[§]Institute of Organic and Polymeric Materials, National Taipei University of Technology, Taipei 10617, Taiwan,

Ⓢ Supporting Information

ABSTRACT: We report the synthesis, morphology, and applications of conjugated rod−coil−coil triblock copolymers, polyfluorene-*block*-poly(*N*-isopropylacrylamide)-*block*-poly(N-methylolacrylamide) (**PF-*b*-PNIPAAm-*b*-PNMA**), prepared by atom transfer radical polymerization first and followed by click coupling reaction. The blocks of PF, PNIPAAm, and PNMA were designed for fluorescent probing, hydrophilic thermo-responsive and chemically cross-linking, respectively. In the following, the electrospun (ES) nanofibers of PF-*b*-PNIPAAm-*b*-PNMA were prepared in pure water using a single-capillary spinneret. The SAXS and TEM results suggested the lamellar structure of the **PF-*b*-PNIPAAm-*b*-PNMA** along the fiber axis. These obtained nanofibers showed outstanding wettability and dimension stability in the aqueous solution, and resulted in a reversible on/off transition on photoluminescence as the temperatures varied. Furthermore, the high surface/volume ratio of the ES nanofibers efficiently enhanced the temperature-sensitivity and responsive speed compared to those of the drop-cast film. The results indicated that the ES nanofibers of the conjugated rod−coil block copolymers would have potential applications for multifunctional sensory devices.

KEYWORDS: electrospinning, thermo-responsive, rod−coil copolymers, chemical cross-linking, luminescence, sensing
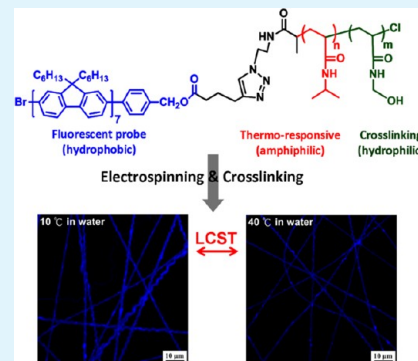
■ INTRODUCTION

Multifunctional copolymers containing π-conjugated rods and environmental-stimulus coils have attracted extensive scientific interest for sensory or biological applications because their nanostructures and photophysical properties could be significantly tuned by external stimuli, such as pH, temperature, light, etc.[1−10] Among the reported environmental-stimulus polymers, poly(*N*-isopropylacrylamide) (PNIPAAm)[11] exhibits the characteristic of lower critical solution temperature (LCST) at 32 °C closely to the human body temperature. It shows a hydrophilic extended structure below the LCST, whereas above the LCST, it dehydrates and forms a compact structure.

Diblock copolymers consisting of PNIPAAm and π-conjugated rod blocks undergo a structural variation above the LCST which leads changes of the optoelectronic properties allowing sensory device applications.[12−14] McCarley et al.[15] reported that a highly water-soluble, thermally responsive poly(thiophene-graft-NIPAAm) (PT-*g*-PNIPAAm) underwent a reversible phase transition from a coiled structure to a collapsed globule with increasing temperature. We developed rod−coil diblock or triblock copolymers with the distinct

variations on the surface structure and their photophysical properties through solvent and temperature stimulus[6,13,16,17] The micellar morphologies of poly[2,7-(9,9-dihexylfluorene)]-*block*-poly(*N*-isopropylacrylamide)-*block*-poly(*N*-(2-hydroxyethyl)acrylamide) changed from worms, to bundles of wormlike micelles, and hollow tubes based on their LCST in aqueous solution, leading to the significant variation on the photoluminescence.[13]

The geometrical confinement and high surface/volume ratio of electrospun (ES) nanofibers could provide further manipulation on the morphology and optoelectronic properties of conjugated rod−coil block copolymers for sensory applications, such as volatile organic compounds,[18,19] gas,[20] pH,[21,22] temperature,[23,24] and biological[25,26] sensors, etc. However, the stimulus-responsive ES nanofibers of conjugated rod−coil block copolymers in aqueous solution have not fully explored yet, which would be important for environmental or

biological applications. Previously, we reported the synthesis and multifunctional sensing characteristics of random copolymer, poly(DMAEMA-co-SA-co-StFl). Because it is a random copolymer, it does not have an ordered morphology as that of conjugated rod−coil block copolymers. In addition, the physically cross-linking moiety of stearyl acrylate (SA) is not relatively stable as the chemically cross-linking poly(N-methylolacrylamide) (PNMA) in water. Thus, the poly-(DMAEMA-co-SA-co-StFl) ES nanofibers would lose their cylindrical shape gradually after several heating/cooling cycles and diminish the speed of responsibility. Furthermore, the main-chain PF-based conjugated rod−coil block copolymers would have stronger photoluminescence intensity because there is only one fluorene moiety in poly(DMAEMA-co-SA-co-StFl).

Herein, we report the synthesis, characterization, and sensory applications of polyfluorene-block-poly(N-isopropylacrylamide)-block-poly(N-methylolacrylamide) (PF-b-PNIPAAm-b-PNMA) and their ES nanofibers, as shown in Scheme 1. The

Scheme 1. Design of Multifunctional Sensory ES Nanofibers from Conjugated Rod−Coil−Coil Triblock Copolymers
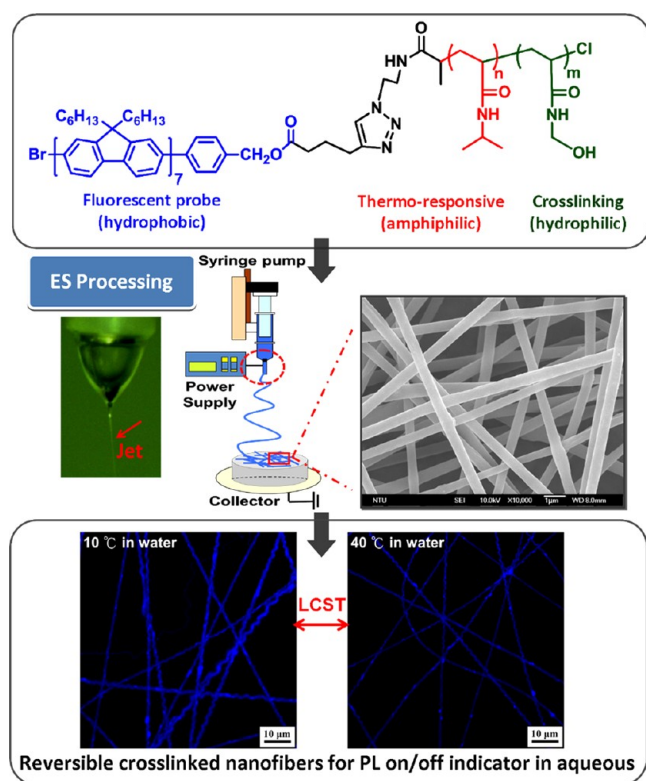
polymers consist of three functional blocks, fluorescent π-conjugated rod (PF), hydrophilic thermoresponsive material (PNIPAAm), and chemically cross-linkable segment (PNMA). As shown in Scheme 2, the triblock copolymers of PF-b-PNIPAAm-b-PNMA were synthesized by atom transfer radical polymerization (ATRP) first and followed by click coupling reaction. The ES nanofibers of PF-b-PNIPAAm-b-PNMA were prepared in pure water with the additive of polyethylene oxide (PEO) by a single-capillary spinneret. In the following, the nanofibers were post-treated to enhance their stability in water by chemical cross-linking and then PEO was extracted from the nanofibers. The LCST, morphology, and stimuli-responsive photoluminescence characteristics of the prepared nanofibers were characterized. The experimental results suggested that the

ES nanofibers prepared from conjugated rod−coil triblock copolymers could have the on/off fluorescence response for multifunctional device applications.

■ EXPERIMENTAL SECTION

Materials. N-Isopropylacrylamide (NIPAAm) and N-hydroxyethylacrylamide (NMA) were provided by Tokyo Chemical Industry Co., Japan, and NIPAAm was recrystallized three times from hexane/toluene (10/1, v/v) prior to use. Tris[2-(dimethylamino)ethyl]amine (Me$_6$TREN) was supplied by Mitsubishi Chemical Co., Japan, and distilled under reduced pressure from calcium hydride, then stored under nitrogen. Copper(I) chloride, copper(I) bromide (98%), and N,N,N',N'',N''-pentamethyldiethylenetriamine (PMDETA) were provided from Aldrich Chemical Co. and used without further purification. N-(2'-Azidoethyl)-2-chloropropionamide (AECP) and alkynyl-terminated polyfluorene (4) were prepared according to our previous report.[13,27] Common organic solvents for synthesis were obtained commercially and used as received unless otherwise noted.

Synthesis of PF-b-PNIPAAm-b-PNMA Rod−Coil−Coil Triblock Copolymers (5). Click reaction between alkynyl-terminated PF and azide-terminated PNIPAAm-b-PNMA blocks were performed according to Scheme 2. Typically, 4 (160 mg, 0.06 mmol), N$_3$−PNIPAAm$_{100}$-b-PNMA$_{50}$ (3b) (480 mg, 0.03 mmol), and CuBr (17 mg, 0.12 mmol) were dissolved by 6:4 THF/DMF (10 mL, v/v) in a dried Schlenk flask. The reaction mixture was evacuated for 30 min and backfilled with argon. Then, PMDETA (25 μL, 0.12 mmol) was added, and the flask was immersed in a preheated oil bath at 50 °C for overnight. The reaction was quenched by exposure to air, diluted with THF, and removed the copper complex through a silica column. The reaction mixture was evaporated at room temperature, and redissolved in water. To remove unreacted reactants completely, we extracted the solution with diethyl ether and dialyzed against THF and water with a KOCH HFM-181 dialysis membrane (molecular weight cutoff of 18 000 g mol^{-1}) for 4 days. Finally, freeze-dried to give polymer PF$_7$-b-PNIPAAm$_{100}$-b-PNMA$_{50}$ (5b) (363 mg, 57%) as a light yellow solid. The GPC analyses using DMF eluent (see Figure S2 in the Supporting Information) showed the single peak without appreciable shoulders/or tailings at the both sides and confirmed that the unreacted reactants were completely removed. ^{1}H NMR in CDCl$_3$, δ (ppm) 0.91−1.45 (6H, −CH(C$\underline{H}$$_3$)$_2$), 1.48−1.93 (2H, −C$\underline{H}$$_2$CH−), 1.94−2.42 (1H, −CH$_2C\underline{H}$−), 3.88−4.14 (1H, −C$\underline{H}$(CH$_3$)$_2$) (2H, −CH$_2CH_2$OH), 3.71−3.94 (2H, −CH$_2CH_2$OH), 3.93−4.16 (1H, −CH(CH$_3$)$_2$), 5.67−6.78 (1H, −CON$\underline{H}$CH−), 7.30−7.89 (10H, fluorene aromatic protons and phenyl group). ^{1}H NMR in DMSO-d$_6$, δ (ppm) 0.84−1.18 (6H, −CH(C$\underline{H}$$_3$)$_2$), 1.25−1.72 (4H, −C$\underline{H}$$_2$CH−, −C$\underline{H}$$_2$CH−), 1.80−2.20 (2H, −CH$_2C\underline{H}$−, −CH$_2C\underline{H}$−), 3.71−3.97 (1H, −C$\underline{H}$(CH$_3$)$_2$), 4.36−4.65 (2H, −CONHC$\underline{H}$$_2$−), 5.34−5.63 (H, −NHCH$_2O\underline{H}$), 6.97−7.59 (1H, −CON$\underline{H}$CH−), 7.97−8.42 (1H, −N$\underline{H}CH_2$OH). $M_{n,GPC (DMF)}$ = 44 800 g mol^{-1}, M_w/M_n = 1.41.

Preparation of Electrospun Nanofibers and Drop-Cast Films. N$_3$−PNIPAAm-b-PNMA and PF-b-PNIPAAm-b-PNMA were dissolved in H$_2$O with the concentration of 80−100 mg/mL for preparing the ES nanofibers. To enhance the polymer entanglement of electrospun solution, 12 wt % (with respect to the block copolymer) of poly(ethylene oxide) (PEO, M_v = 400 000) was added. A single-capillary spinneret ES device was employed to produce the ES nanofibers, similar to our previous report.[28] The polymer solution was fed into the metallic needle by syringe pumps (KD Scientific Model 100, USA), and maintained the feed rate of 0.8−1.0 mL/h. The tip of metallic needle was connected to a high-voltage power supply (Chargemaster CH30P SIMCO, USA), and set at 15 KV during whole ES process. A piece of aluminum foil or quartz was placed 15 cm below the tip of the needle to collect ES nanofibers for 2 h. All experiments were carried out at room temperature under about 50% of the relative humidity.

For the comparison with the properties of the ES nanofibers, the corresponding polymer films were drop-cast on a glass substrate from the same polymer solutions and dried in an airflow hood.

Scheme 2. Synthesis of PF-b-PNIPAAm-b-PNMA Rod−Coil−Coil Triblock Copolymers
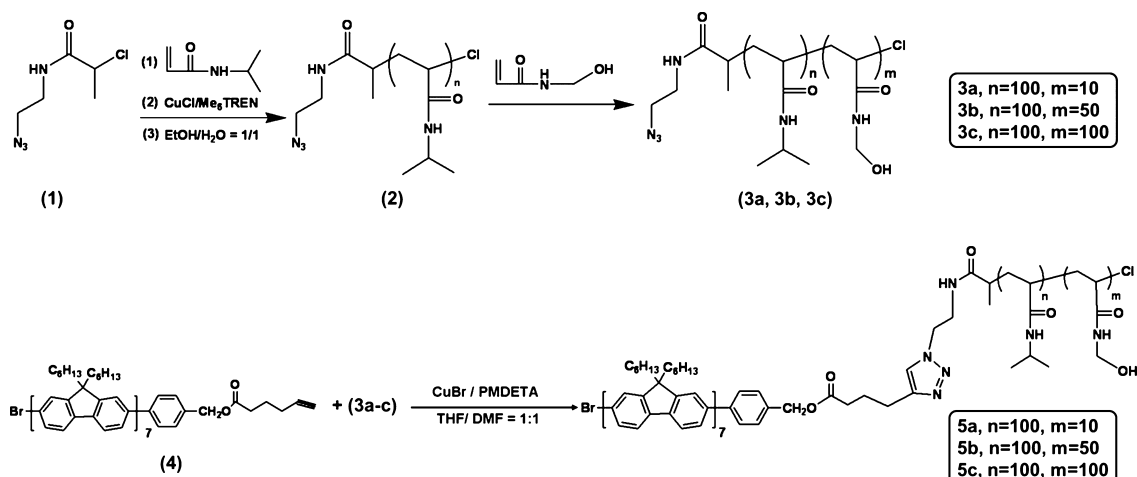
Characterization.

Lower critical solution temperature (or volume phase transition) of the cross-linked electrospun mats were carried out on a differential scanning calorimetry (DSC) from TA Instruments (TA Q100) with heating cycle from 20 to 60 °C at the heating rate of 2 °C/min.

Small-angle X-ray scattering (SAXS) measurements of pure PF-b-PNIPAAm-b-PNMA were carried out with graphite-monochromatized Cu KR radiation using a Bruker diffractometer (NanoSTAR Universal System). SAXS data were collected on beamline BL23A1 in the National Synchrotron Radiation Research Center (NSRRC), Taiwan. A monochromatic beam of λ = 0.887 Å was used.[29] The scattering intensity profiles were reported as the plots of the scattering intensity (I) vs the scattering vector q, where q=$(4\pi/\lambda)\sin(\theta/2)$, θ is the scattering angle.

The setup on measuring the photoluminescence spectra of the ES nanofibers and drop-cast films at different temperatures is shown in Figure S3 of the Supporting Information. To ensure that the beam excites at the specific location on the nanofiber mats at every measurement, the samples were fixed in cuvettes by adhesive tape and filled with pure water, then heated or cooled by a circulating water bath between 10 and 50 °C in an interval of 5 °C every 10 min. All photoluminescence spectra of the ES fibers and drop-cast films were also recorded on Fluorolog-3 spectrofluorometer (Horiba Jobin Yvon) excited at the wavelength of 370 nm, as described in our previous study.[23,28]

The morphologies of ES nanofibers were performed through field-emission scanning electron microscope (FE-SEM, JEOL JSM-6330F) and transmission electron microscopy (TEM, JEOL 1230). In the TEM study, The ES nanofibres were first sputtered with platinum on the surface for realizing the fiber location in observation, and embedded by epoxy, then microtomed using a diamond knife. Subsequently, specimens were stained by exposing to the vapor of ruthenium tetroxide (RuO$_4$). Fluorescence optical microscope images were taken using two-photon laser confocal microscope (Leica LCS SP5) with a water bath holder.

■ RESULTS AND DISCUSSION

Polymer Structure Characterization. The successful synthesis of diblock copolymers with the terminal azido group, N$_3$−PNIPAAm$_{100}$-b-PNMA$_{10}$ (**3a**), N$_3$−PNIPAAm$_{100}$-b-PNMA$_{50}$ (**3b**), and N$_3$−PNIPAAm$_{100}$-b-PNMA$_{100}$ (**3c**), was evidenced by the NMR spectra (see Figure S4 in the Supporting Information). The number-average molecular weights of the copolymers **3a**–**3c** estimated from GPC are 25400, 32900, and 36800 g mol^{-1}, with the corresponding polydispersity indices of 1.31, 1.42, and 1.46 (see Table S1 and Figure S1 in the Supporting Information), respectively.

The coupling between PF and PNIPAAm-b-PNMA was characterized by FTIR, GPC, and ^{1}H NMR. As observed from the FTIR spectra of copolymers **3b** and **5b** (see Figures S2 and S5 in the Supporting Information), the terminal azido group of polymer **3b** confirmed by the peak at 2104 cm^{-1} is disappeared completely in the spectrum of copolymer **5b**. It suggests the successful click coupling between azido and alkyne groups. The ^{1}H NMR spectra of a PF$_7$-b-PNIPAAm$_{100}$-b-PNMA$_{50}$ (**5b**) in CDCl$_3$ and DMSO-d_6 are also shown in Figure S5 in the Supporting Information. The aromatic proton signals from fluorene and the triazole ring of the copolymer **5b** appear in the range of 7.30−7.89 ppm in CDCl$_3$, but it could not observe the methine, methylene, and hydroxyl proton peaks of hydrophilic PNMA due to its limited solubility in CDCl$_3$. Therefore, we employed another hydrophilic d-solvent, DMSO-d_6, to further examine ^{1}H NMR peaks. In a sharp contrast, the spectrum in DMSO-d_6 shows the existence of the hydrophilic N$_3$−PNIPAAm-b-PNMA (**3**) proton peaks but completely loses the fluorene proton signals. The disappearance of the hydrophobic fluorene block in NMR spectrum is due to the limited mobility of the hydrophobic core in hydrophilic d-solvent.[30,31] This phenomenon is also observed in the NMR and IR spectra of PF$_7$-b-PNIPAAm$_{100}$-b-PNMA$_{10}$ (**5a**) and PF$_7$-b-PNIPAAm$_{100}$-b-PNMA$_{100}$ (**5c**) (see Figures S6 and S7 in the Supporting Information). GPC analyses of PF-b-PNIPAAm-b-PNMA in dimethylformamide (DMF) reveal monomodal and symmetric peaks. The number-average molecular weights of copolymers **5a**−**5c** are 30 700, 44 800, and 47 500 g mol^{-1}, respectively, with the polydispersity indices of 1.33, 1.41, and 1.52, as listed in Table 1. The above results suggest the successful preparation of the targeted PF-b-PNIPAAm-b-PNMA (**5**) triblock copolymers.

The thermal decomposition temperatures (T_d) of the copolymers, **5a**, **5b**, and **5c**, estimated from TGA (Table 1) are 326, 309, and 301 °C (see Figure S8 in the Supporting Information), which decrease with the increased segment length of PNMA. On the other hand, the glass transition temperature (T_g) of **5a**, **5b**, and **5c**, estimated by DSC (see Figure S9 in the Supporting Information) are 128, 132, and 135 °C, respectively. The increase on the T_g is resulted from the incorporation of the PNMA moiety.[32] Figure 1 shows the typical optical transmittance (at 600 nm) vs. temperature curves of **5a**−**5c** in water. The lower critical solution temperature (LCST) of copolymers **5a**, **5b**, and **5c** estimated

Table 1. Molecular Weights and Thermal Properties of PF$_7$-b-PNIPAAm-b-PNMA (5) Triblock Copolymers

| polymer[a]	$M_{n\ GPC}$[b] (M_w/M_n)	T_g (°C)	T_d[c] (°C)	LCST (°C)
PF$_7$-b-PNIPAAm$_{100}$-b-PNMA$_{10}$ (5a)	30 700 (1.33)	128	326	34
PF$_7$-b-PNIPAAm$_{100}$-b-PNMA$_{50}$ (5b)	44 800 (1.41)	132	309	40
PF$_7$-b-PNIPAAm$_{100}$-b-PNMA$_{100}$ (5c)	47 500 (1.52)	135	301	46

[a]Feed molar ratio (2/1) of the alkynyl-terminated PF [PF]$_0$ to PNIPAAm-b-PNMA [diblock]$_0$. [b]Determined by GPC with DMF eluent. [c]Onset decomposition
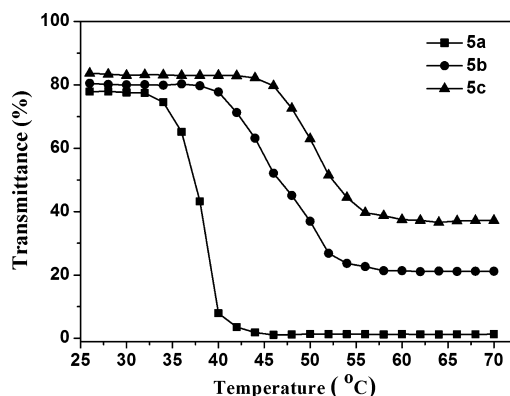
Figure 1. Variation in optical transmittance in water with temperature (25−70 °C) of PF-b-PNIPAAm-b-PNMA (5).

from Figure 1 are 34, 40, and 46 °C, respectively. The incorporation of the hydrophilic segment, PNMA, retains polymer chains to stretch at an elevated temperature and thus enhances the LCST.

Electrospun Nanofibers of PF-b-PNIPAAm-b-PNMA. We attempted to produce electrospun nanofibers of PF-b-PNIPAAm-b-PNMA, but failed neither by adjusting the copolymer concentration nor changing solvent (H$_2$O or MeOH/H$_2$O). It suggested that there was not enough entanglement in the olymer solution because the molecular weights of the prepared polymers were not high. Therefore, water-soluble high-molecular-weight polyethylene oxide (PEO) was added to enhance the solution viscosity for obtaining the ES fibers and then it could be removed by water extraction after cross-linking of NMA segment. Figure 2 shows the SEM image of the ES nanofibers prepared from the 12 wt % of 5/PEO polymer blends in aqueous solutions. The diameters of the electrospun fibers from polymer blends 5a/PEO, 5b/PEO, and 5c/PEO are 358 ± 68, 486 ± 61, and 524 ± 93 nm. Note that the average fiber diameter was estimated based on a statistical average of fifty fibers from each sample. The increased average diameter of as-spun fibers from 358 to 524 nm is due to the enhanced polymer molecular weights.[33,34] In this study, the PNMA block was employed to provide the cross-linking structure by thermal catalyzed reaction, which first formed bis(methylene ether) by loss of water and then the methylene bridge by the loss of formaldehyde.[35] Then, the prepared nanofibers were cross-linked by heating at 80 °C in an oven under atmosphere. After cross-linking, the fiber mats were flushed by water about 6−8 times at 30 °C and then dried at same temperature under vacuum. Figure 3 shows the SEM images of the ES nanofibers at different cross-linking time on
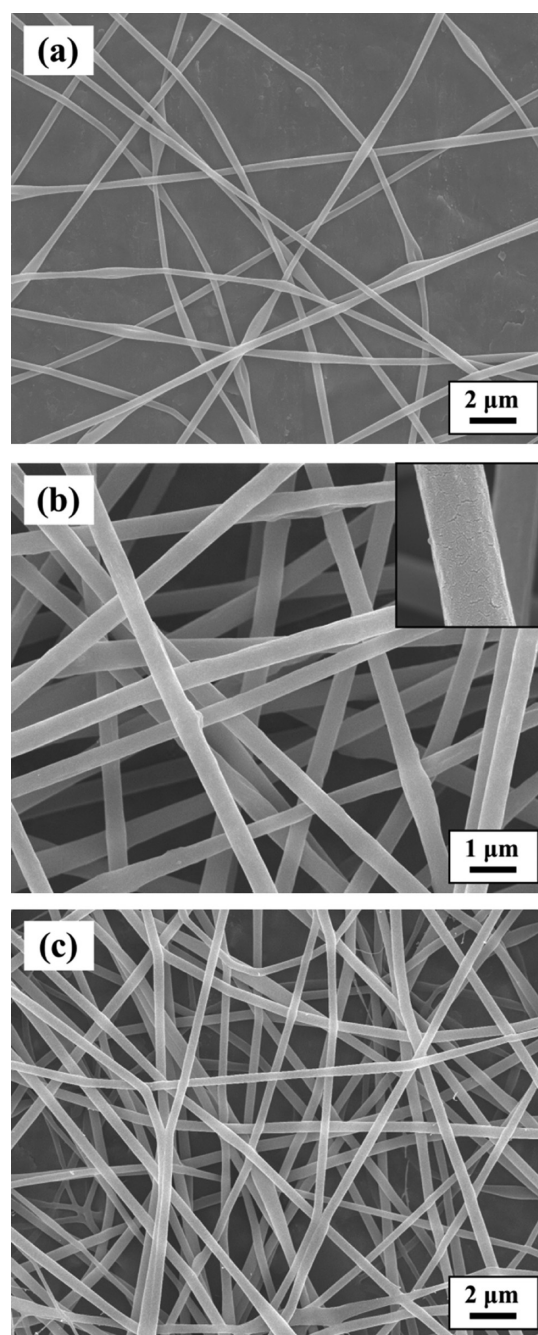
Figure 2. FE-SEM images of ES nanofibers from 10 wt % copolymer in H$_2$O solution: (a) 5a/PEO, (b) 5b/PEO, and (c) 5c/PEO.

80 °C. In Figure 3, ES nanofibers of copolymer 5a show a smooth surface (8 h), to a crispy film (48 h) and a flat film (96 h) after extracting by water. It suggests that the cross-linked PNMA block with 10 repeat units could resist the solubility of water but could not maintain a stable fiber shape. With increasing the block length of the cross-linkable NMA, ES nanofibers of copolymers 5b and 5c (Figure 3) retain the cylindrical fiber shape after extraction of water, with the cross-linking time more than 48 h. It indicates that the stability of nanofibers is enhanced with increasing the PNMA block length and cross-linking time.[37] On the other hand, the diameter of cross-linked PF$_7$-b-PNIPAAm$_{100}$-b-PNMA$_{50}$ nanofibers after extraction is about 370 nm, which is smaller than as-spun fibers (486 ± 61 nm) with a more rough surface (see Figure
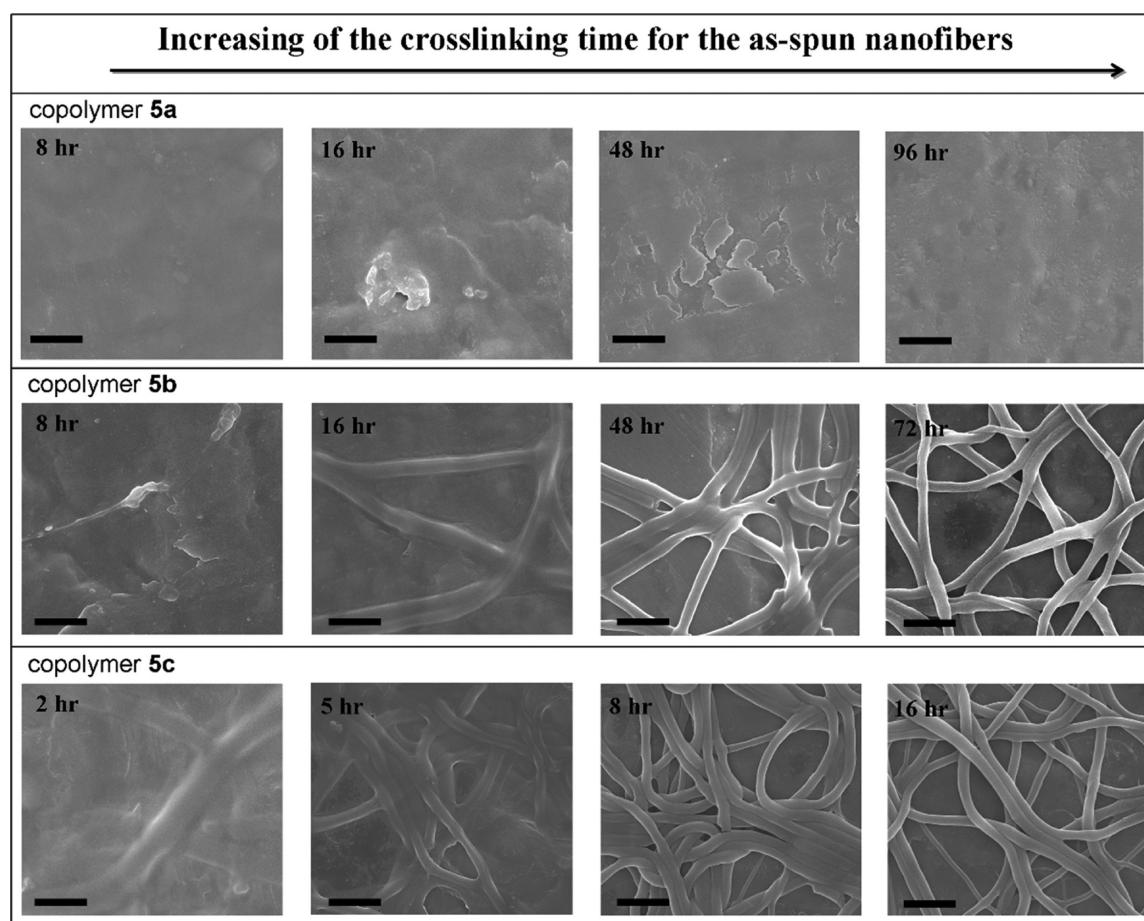
Figure 3. FE-SEM images of copolymers, **5a**, **5b**, and **5c** nanofibers cross-linked at 80 °C with variation time and treated by water at 30 °C (all scale bars are 2 μm).

S10 in the Supporting Information), mostly due to the extraction of PEO by water. Furthermore, the cross-linked **5b** nanofibers still maintain well-defined cylindrical shape after immersed in water at room temperature for a week. Similar stability of the ES nanofibers in aqueous solution was also found on copolymer **5c** after cross-linking. These results reveal excellent stability of the prepared cross-linked nanofibers to the water environment.

The morphology of the ES nanofibers prepared from block copolymers showed different structure as those of drop-cast film.[36−39] Here, SAXS and TEM were used to characterize the detailed morphology of the cross-linked ES nanofibers. Figure 4a shows the cross-sectional TEM image of the ES nanofibers prepared from copolymer **5b**, which shows the lamellar-like structure along the fiber axis. Note that the darker regions are attributed to the PF block due to the staining of RuO_4. We further investigated the morphology of the prepared ES nanofibers by SAXS and showed a shoulder around 0.027 $Å^{-1}$, corresponding to a spacing ~23.2 nm (see Figures S11 and 12 in the Supporting Information). Besides, we investigated the SAXS pattern of the copolymer **5b** drop-cast film to support the TEM result of the ES nanofibers, which exhibited the diffraction peak positions of 1:2:3:4. It implies lamellar structures with a d-spacing of 33.7 nm estimated from the first order peak at q = 0.019 $Å^{-1}$ (Figure 4b). Thus, we confirm that the lamellar structures of the triblock copolymer, **5b**, within the ES nanofibers, and the interior structure of cross-linked nanofibers is shown in Figure 4c. The formation of the

lamellar structure in both cross-linked film and nanofibers could be due to the strong π−electron interaction between the PF block or the microphase separation between of the PF and PNIPAAM/PNMA. On the other hand, the orientation along the fiber axis and smaller d-spacing in nanofibers than that of drop-cast film is probably resulted from the strong "shear forces" provided by the electric filed during electrospinning.

Thermoresponsive Characteristics of the Cross-Linked ES Nanofibers. The LCST of cross-linked ES nanofiber mats was estimated by DSC. The endothermic peak indicates the destruction of the hydrogen-bonding between PNIPAAm block and water molecules with elevating temperature. The LCST of copolymers **5b** and **5c** shown in Figure 5 are 35.9 and 39.1 °C, respectively, which are lower than those in solution due to the cross-linked PNMA segment.[40]

As reported in the literatures,[23,41] the ES nanofiber containing thermoresponsive PNIPAAm or PDMAEMA with physically cross-linked SA moiety exhibited swollen and shrunk characteristics below or above their LCST. To observe the cross-linked ES nanofibers morphology with varying temperature in pure water, the ES nanofibers of copolymer **5b** and **5c** were immersed in water at 20 or 50 °C, respectively. After 5 min, the samples were picked into a flask containing liquid nitrogen to solidify them instantly. Then, the residual water immediately was removed under vacuum for 30 min to retain the original morphology. Figure 6 shows the SEM images of the cross-linked **5b** nanofibers prepared from the above procedures.
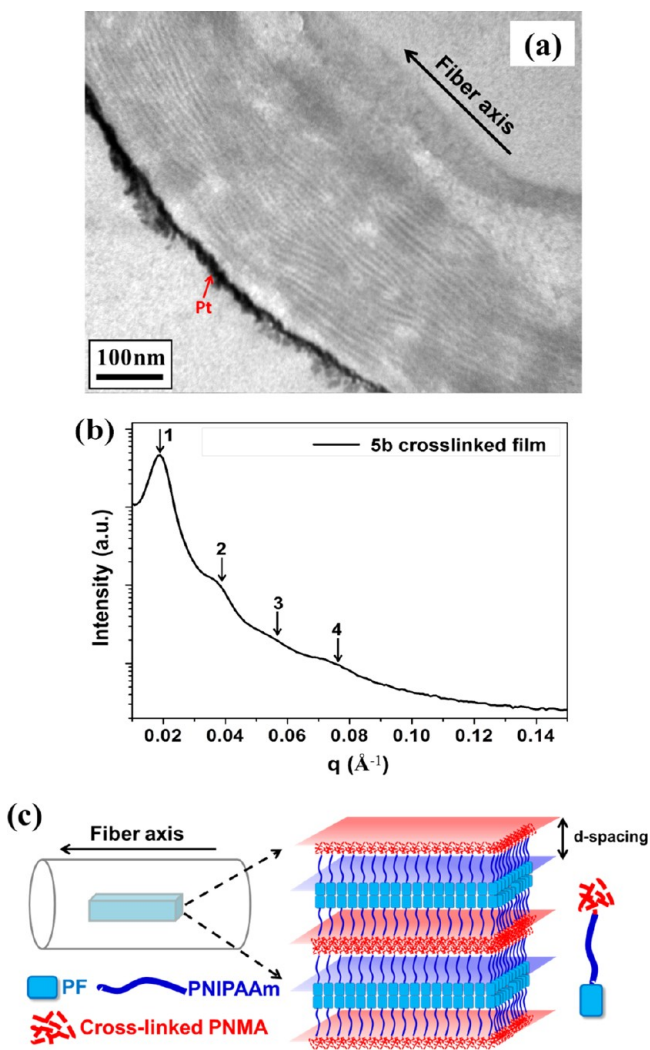
Figure 4. (a) Cross-sectional TEM images of **5b** cross-linked nanofibers . (b) SAXS data of **5b** cross-linked film. (c) Illustration of the interior morphology of **5b** cross-linked nanofibers.

Compare to the morphology at 50 °C, the nanofiber structure is significantly swollen in water at 20 °C due to the hydrophilic PNIPAAm moiety. However, these swollen nanofibers still maintain their cylindrical shape and do not dissolve in water at 20 °C, due to the chemically cross-linked PNMA moiety. On the other hand, the nanofiber diameter is reduced from 512 ± 43 nm to 343 ± 39 nm (Figure 6a, b) as the temperature is increased from 20 to 50 °C, which reveals a shrunk state. Such volume variation is due to the water expelling from the ES fibers as the temperature exceeds the LCST. In the case of a higher PNMA content (see Figure 13 in the Supporting Information), the **5c** ES nanofibers exhibit a slighter swollen/ shrunk state between 20 and 50 °C in water, than that of **5b** ES nanofibers. It suggests that the high content of the chemically cross-linking PNMA effectively restrains its swollen/shrunk characteristics of the prepared ES nanofibers.

Photoluminescence of Cross-linked PF-*b*-PNIPAAm-*b*-PNMA ES Nanofibers. Figure 7 shows the variation on the PL spectra of the cross-linked **5b** ES nanofibers and their corresponding films using the temperature heating/cooling cycle from 10 to 50 °C. The PL spectra of the ES nanofibers exhibit the main emission peak at (425, 446) nm with a shoulder at 475 nm, attributed to the polyfluorene block. As the
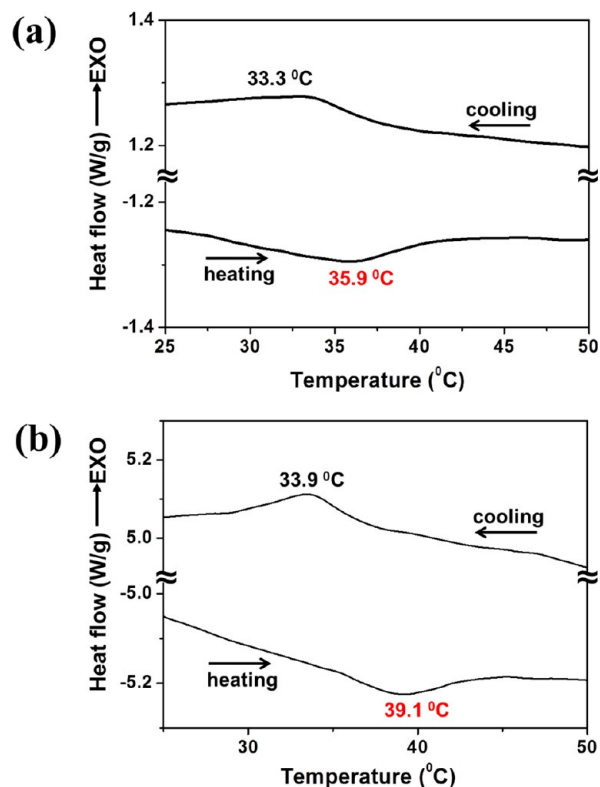

Figure 5. DSC thermograms of the cross-linked ES nanofiber mats (a) **5b** and (b) **5c**.
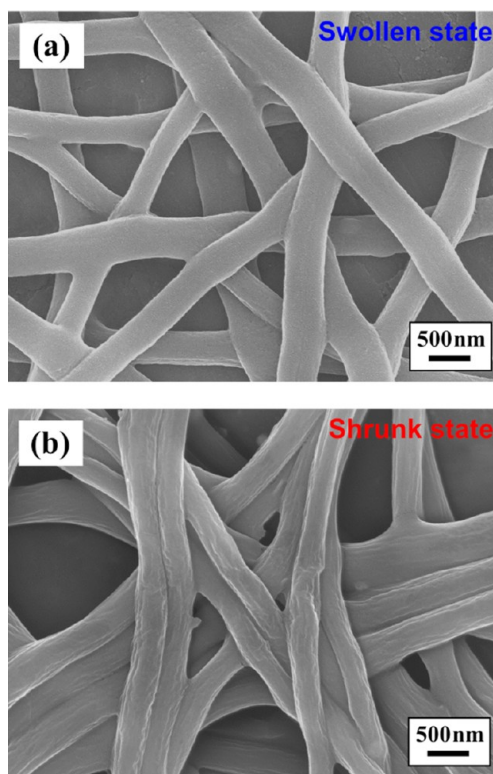

Figure 6. FE-SEM images of the **5b** cross-linked nanofibers treated by water as temperature varied from (a) 20 to (b) 50 °C.

temperature increased from 10 to 50 °C, a significant quenching on the PL intensity of the **5b** ES nanofibers is observed in Figure 7a. After a heating process, a cooling process
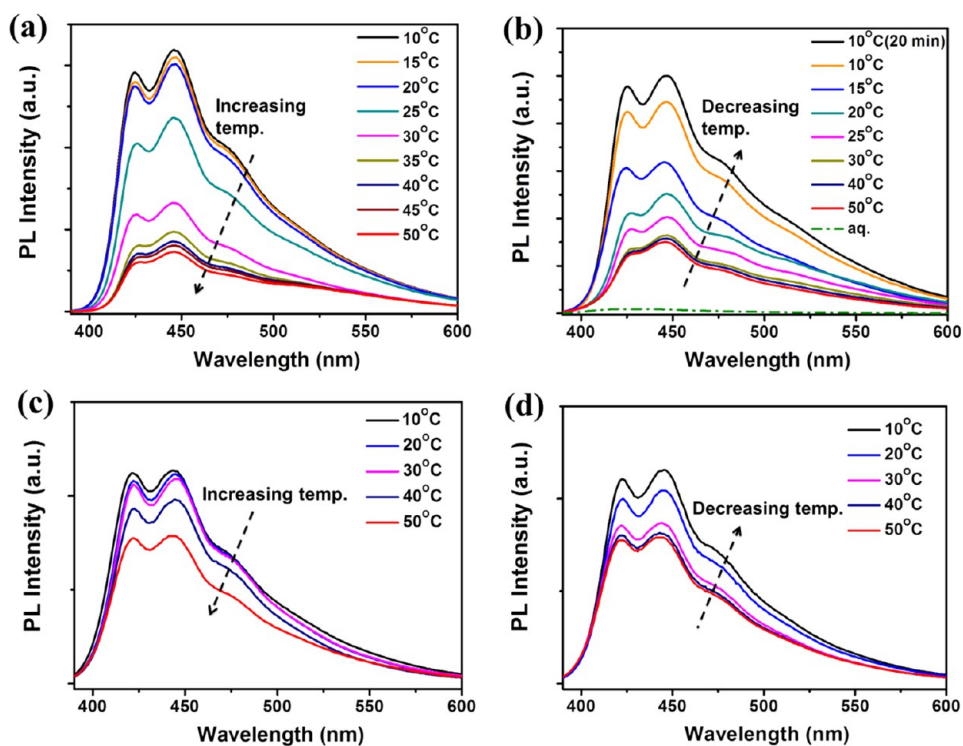
3392

dx.doi.org/10.1021/am300315v | ACS Appl. Mater. Interfaces 2012, 4, 3387–3395

Figure 7. Photoluminescent spectra of **5b** both cross-linked ES nanofibers and drop-cast films in the temperature range of 10−50 °C: increasing temperature and reverse process of (a, b) nanofiber mat, (c, d) drop-cast films. (Note all samples are excited at the wavelength of 370 nm.)
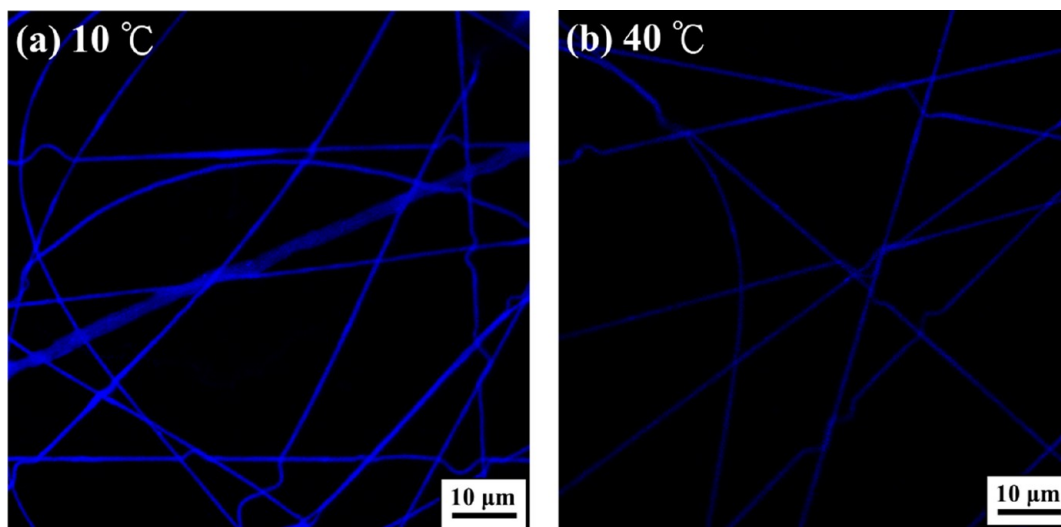

Figure 8. Confocal images of cross-linked **5b** nanofibers immersed in pure water between (a) 10 and (b) 40 °C.

is stimulated to the nanofibers instantly and the emission intensity increases again, as shown in Figure 7b. In the reversible cycle, the emission intensity during the cooling process is less than that of the heating process under the same stimulus condition. Such hysteresis is due to the formation of intra- and interchain hydrogen bonds between different PNIPAAm segments when they are overlapped in the collapsed state.[42,43] On the sharp contrast, the PL intensity changes only slightly between 10 and 50 °C in the corresponding drop-cast film of **5b** compared to that of the ES nanofiber mats (Figure 7c, d). It suggests that the prepared ES nanofibers with the high surface/volume ratio enhances the responsibility (up to 4 times) and sensitivity significantly in the temperature range of 10−50 °C, much higher than those of the drop-cast film.

The above thermoreversible luminescence characteristics could be correlated with the morphological changes induced by temperature, as described in the following. At the temperatures below LCST, the hydrophilic C=O and N−H groups of the PNIPAAm blocks interact with water molecules through hydrogen bonds. Therefore, the PNIPAAm blocks are swollen and the incident light can be absorbed by the PF blocks, which results in a stronger PL luminescence. Once the temperature is increased above LCST, the water molecules are squeezed out from the PNIPAAm block because of the weakening of intermolecular hydrogen bonds and the PNIPAAm chains collapse. As a result, the shrunk PNIPAAm layers suppress the absorption of light in the PF blocks, therefore leading to the PL quenching. In addition, the shrunk

PNIPAAm could lead to the aggregation of the PF moiety and result in the PL quenching.[44]

For the higher composition of the cross-linked NMA moiety, **5c** nanofiber mat (see Figure 14 in the Supporting Information), the PL variation during the heating/cooling cycles resembles with the **5b** case. However, the difference on the responsive intensity is smaller than that of the **5b** mat due to the limited chain movement of the higher cross-linked structure. Obviously, the **5c** nanofiber mat also has a much better thermoresponsive performance than the corresponding film. In addition, both of the nanofiber mats maintain a well-defined fiber structure after the heating−cooling cycle (see Figure 15 in the Supporting Information).

The variation in the PL intensity with heating/cooling cycle was further imaged in water instantaneously by the laser confocal microscope. Cross-linked nanofibers collected on the quartz substrate were immersed in an incubator filled up with water and recorded the real time images when the temperature arrives to equilibrium. As shown in Figure 8, the **5b** cross-linked nanofiber maintain the cylindrical shape in water at 40 °C or even at 10 °C. Besides, the blue light emission of cross-linked fibers in water show bright blue emission at 10 °C but it is significantly quenched at 40 °C. The change on the volume and PL intensity of **5b** ES nanofibers is more distinct than that of **5c** (see Figure 16 in the Supporting Information), which is consistent with the PL result.

The time-dependent variation in the PL intensity on the **5b** nanofibers with the heating−cooling cycle is shown in Figure 9.
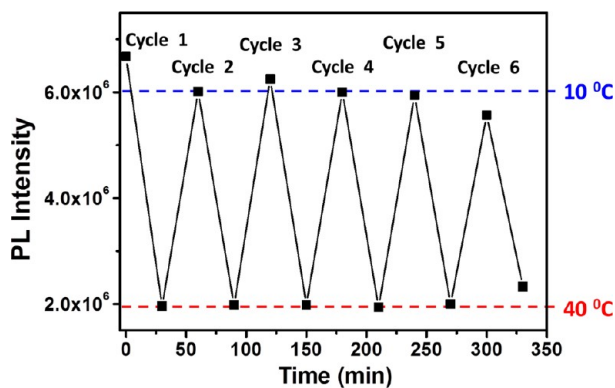

Figure 9. Reversibility of time-dependent "on−off−on" fluorescence intensity profile of the cross-linked **5b** nanofiber mat.

Significantly, **5b** nanofibers mat exhibits a rapid PL response when applied certain temperature and could be repeated for several times. However, the shrunk PNIPAAM could not be fully recovered back to the original state due to hysteresis phenomenon and lead to the PL deviation in the cooling processes form cycle 2 to cycle 6. Those results reveal the excellent sensitivity and stability to environmental stimuli of the ES nanofibers prepared the multifunctional triblock copolymers.

CONCLUSIONS

We have successfully prepared conjugated rod−coil−coil triblock copolymers of PF-*b*-PNIPAAm-*b*-PNMA and their electrospun nanofibers, which are consisted of photoluminescence, thermoresponsive and chemical cross-linking block. The cross-linked nanofiber mats with the lamellar structure showed outstanding wettability and integrity in aqueous solution, and

had a reversible on/off photoluminescence transition at various temperatures. At the temperature below LCST, the PNIPAAm blocks were swollen and the incident light could be absorbed by the PF blocks, leading to a stronger PL luminescence. Once the temperature was increased above the LCST, the shrunk PNIPAAm layers suppressed the light absorption of the PF blocks or induced large PF aggregated domain, which led to the PL quenching. Besides, the high surface/volume ratio of the ES nanofibers efficiently enhanced the sensitivity and responsive speed to temperature compared to the corresponding drop-cast film. The results indicated that the ES nanofibers of the conjugated rod−coil block copolymers would have potential applications for multifunctional sensory devices.

ASSOCIATED CONTENT

Ⓢ Supporting Information

Polymerization conditions and molecular weights of N_3−PNIPAAm-*b*-PNMA (**3**) diblock copolymers. GPC profiles of copolymers, **3a**, **3b**, **3c**, **5a**, **5b**, and **5c**. The setup for the analysis of photoluminescence measurements with various temperatures. ^{1}H NMR spectra of copolymerrs, **3a**, **3b**, **3c**, and **5a**, **5b**. IR spectra of copolymers, **3a**, **3b**, **5a**, and **5b**. TGA and DSC curves of copolymers, **5a**−**5c**. Enlarged TEM images of (**5b**)/PEO ES nanofibers. Photoluminescence and confocal images of cross-linked **5c**. This material is available free of charge via the Internet at http://pubs.acs.org.

AUTHOR INFORMATION

Corresponding Author

*E-mail: chenwc@ntu.edu.tw (W.C.C.); kakuchi@poly-bm.eng.hokudai.ac.jp) (T.K.).

Notes

The authors declare no competing financial interest.

REFERENCES

(1) Liu, F.; Urban, M. W. *Prog. Polym. Sci.* **2010**, *35*, 3−23.

(2) Thomas, S. W.; Joly, G. D.; Swager, T. M. *Chem. Rev.* **2007**, *107*, 1339−1386.

(3) Wolfbeis, O. S. *J. Mater. Chem.* **2005**, *15*, 2657−2669.

(4) Liu, C. L.; Lin, C. H.; Kuo, C. C.; Lin, S. T.; Chen, W. C. *Prog. Polym. Sci.* **2011**, *36*, 603−637.

(5) Wu, W. C.; Tian, Y.; Chen, C. Y.; Lee, C. S.; Sheng, Y. J.; Chen, W. C.; Jen, A. K. Y. *Langmuir* **2007**, *23*, 2805−2814.

(6) Lin, S. T.; Tung, Y. C.; Chen, W. C. *J. Mater. Chem.* **2008**, *18*, 3985−3992.

(7) Iwai, K.; Matsumura, Y.; Uchiyama, S.; de Silva, A. P. *J. Mater. Chem.* **2005**, *15*, 2796−2800.

(8) Wang, D.; Miyamoto, R.; Shiraishi, Y.; Hirai, T. *Langmuir* **2009**, *25*, 13176−13182.

(9) Nagai, A.; Kokado, K.; Miyake, J.; Cyujo, Y. *J. Polym. Sci., Part A: Polym. Chem.* **2010**, *48*, 627−634.

(10) Zhou, X.; Su, F.; Gao, W.; Tian, Y.; Youngbull, C.; Johnson, R. H.; Meldrum, D. R. *Biomaterials* **2011**, *32*, 8574−8583.

(11) Gil, E. S.; Hudson, S. M. *Prog. Polym. Sci.* **2004**, *29*, 1173−1222.

(12) Xiao, X.; Fu, Y.-Q.; Zhou, J.-J.; Bo, Z.-S.; Li, L.; Chan, C. M. *Macromol. Rapid Commun.* **2007**, *28*, 1003−1009.

(13) Lin, S. T.; Fuchise, K.; Chen, Y.; Sakai, R.; Satoh, T.; Kakuchi, T.; Chen, W. C. *Soft Matter* **2009**, *5*, 3761−3770.

(14) Tian, Y.; Chen, C. Y.; Yip, H. L.; Wu, W. C.; Chen, W. C.; Jen, A. K. Y. *Macromolecules* **2010**, *43*, 282−291.

(15) Balamurugan, S. S.; Bantchev, G. B.; Yang, Y. M.; McCarley, R. L. *Angew. Chem., Int. Ed.* **2005**, *44*, 4872−4876.

(16) Lin, C. H.; Tung, Y. C.; Ruokolainen, J.; Mezzenga, R.; Chen, W. C. *Macromolecules* **2008**, *41*, 8759−8769.

(17) Huang, K. K.; Fang, Y. K.; Hsu, J. C.; Kuo, C. C.; Chang, W. H.; Chen, W. C. *J. Polym. Sci., Part A: Polym. Chem.* **2011**, *49*, 147−155.

(18) Yoon, J.; Chae, S. K.; Kim, J. M. *J. Am. Chem. Soc.* **2007**, *129*, 3038−3039.

(19) Yoon, J.; Jung, Y.-S.; Kim, J.-M. *Adv. Funct. Mater.* **2009**, *19*, 209−214.

(20) Yang, D. J.; Kamienchick, I.; Youn, D. Y.; Rothschild, A.; Kim, I. D. *Adv. Funct. Mater.* **2010**, *20*, 4258−4264.

(21) Kuo, C. C.; Tung, Y. C.; Chen, W. C. *Macromol. Rapid Commun.* **2010**, *31*, 65−70.

(22) Medina-Castillo, A. L.; Fernandez-Sanchez, J. F.; Fernandez-Gutierrez, A. *Adv. Funct. Mater.* **2011**, *21*, 3488−3495.

(23) Chiu, Y. C.; Kuo, C. C.; Hsu, J. C.; Chen, W. C. *ACS Appl. Mater. Interfaces* **2010**, *2*, 3340−3347.

(24) Tzeng, P.; Kuo, C. C.; Lin, S. T.; Chiu, Y. C.; Chen, W. C. *Macromol. Chem. Phys.* **2010**, *211*, 1408−1416.

(25) Bhattacharyya, D.; Senecal, K.; Marek, P.; Senecal, A.; Gleason, K. K. *Adv. Funct. Mater.* **2011**, *21*, 4328−4337.

(26) Wang, X.; Kim, Y. G.; Drew, C.; Ku, B. C.; Kumar, J.; Samuelson, L. A. *Nano Lett.* **2004**, *4*, 331−334.

(27) Narumi, A.; Fuchise, K.; Kakuchi, R.; Toda, A.; Satoh, T.; Kawaguchi, S.; Sugiyama, K.; Hirao, A.; Kakuchi, T. *Macromol. Rapid Commun.* **2008**, *29*, 1126−1133.

(28) Kuo, C. C.; Lin, C. H.; Chen, W. C. *Macromolecules* **2007**, *40*, 6959−6966.

(29) Sun, H. S.; Lee, C. H.; Lai, C. S.; Chen, H. L. *Soft Matter* **2011**, *7*, 4198−4206.

(30) Zhang, W.; Jiang, X.; He, Z.; Xiong, D.; Zheng, P.; An, Y.; Shi, L. *Polymer* **2006**, *47*, 8203−8209.

(31) Heald, C. R.; Stolnik, S.; Kujawinski, K. S.; De Matteis, C.; Garnett, M. C.; Illum, L.; Davis, S. S.; Purkiss, S. C.; Barlow, R. J.; Gellert, P. R. *Langmuir* **2002**, *18*, 3669−3675.

(32) Fang, Y.; Chen, L.; Chen, S. *J. Polym. Sci., Part A: Polym. Chem.* **2009**, *47*, 1136−1147.

(33) Li, D.; Xia, Y. *Adv. Mater.* **2004**, *16*, 1151−1170.

(34) Greiner, A.; Wendorff, J. H. *Angew. Chem., Int. Ed.* **2007**, *46*, 5670−5703.

(35) Krishnan, S.; Klein, A.; El-Aasser, M. S.; Sudol, E. D. *Macromolecules* **2003**, *36*, 3511−3518.

(36) Ma, M.; Krikorian, V.; Yu, J. H.; Thomas, E. L.; Rutledge, G. C. *Nano Lett.* **2006**, *6*, 2969−2972.

(37) Ma, M.; Titievsky, K.; Thomas, E. L.; Rutledge, G. C. *Nano Lett.* **2009**, *9*, 1678−1683.

(38) Kalra, V.; Kakad, P. A.; Mendez, S.; Ivannikov, T.; Kamperman, M.; Joo, Y. L. *Macromolecules* **2006**, *39*, 5453−5457.

(39) Chen, X.; Dong, B.; Wang, B.; Shah, R.; Li, C. Y. *Macromolecules* **2010**, *43*, 9918−9927.

(40) Ghugare, S. V.; Chiessi, E.; Fink, R.; Gerelli, Y.; Scotti, A.; Deriu, A.; Carrot, G.; Paradossi, G. *Macromolecules* **2011**, *44*, 4470−4478.

(41) Okuzaki, H.; Kobayashi, K.; Yan, H. *Macromolecules* **2009**, *42*, 5916−5918.

(42) Sun, B.; Lin, Y.; Wu, P.; Siesler, H. W. *Macromolecules* **2008**, *41*, 1512−1520.

(43) Cheng, H.; Shen, L.; Wu, C. *Macromolecules* **2006**, *39*, 2325−2329.

(44) Lin, W. J.; Chen, W. C.; Wu, W. C.; Niu, Y. H.; Jen, A. K. Y. *Macromolecules* **2004**, *37*, 2335−2341.